Spectroscopic and Quantum Chemical Evidence of Amine–CO_2 and Alcohol–CO_2 Interactions

Confirming an Intriguing Affinity of CO_2 to Monoethanolamine (MEA)

Yazdabadi, Sahar Hafizi; Mihrin, Dmytro; Feilberg, Karen Louise; Larsen, René Wugt

Published in:
Molecules

Link to article, DOI:
10.3390/molecules29235521

Publication date:
2024

Document Version
Publisher's PDF, also known as Version of record

molecules

MDPI

Article

Spectroscopic and Quantum Chemical Evidence of Amine–CO_2 and Alcohol–CO_2 Interactions: Confirming an Intriguing Affinity of CO_2 to Monoethanolamine (MEA)

Sahar Hafizi Yazdabadi [1,2], Dmytro Mihrin [1,2], Karen Louise Feilberg [2] and René Wugt Larsen [1,*]

[1] Department of Chemistry, Technical University of Denmark, Kemitorvet 206, 2800 Kongens Lyngby, Denmark
[2] DTU Offshore, Technical University of Denmark, Elektrovej 375, 2800 Kongens Lyngby, Denmark
* Correspondence: rewl@kemi.dtu.dk

Abstract: A recent broadband rotational spectroscopic investigation of the cross-association mechanisms of CO_2 with monoethanolamine (MEA) in molecular beams [F. Xie et al., *Angew. Chem. Int. Ed.*, **2023**, *62*, e202218539] revealed an intriguing affinity of CO_2 to the hydroxy group. These findings have triggered the present systematic vibrational spectroscopic exploration of weakly bound amine··CO_2 and alcohol··CO_2 van der Waals cluster molecules embedded in inert "quantum" matrices of neon at 4.2 K complemented by high-level quantum chemical conformational analyses. The non-covalent interactions formed between the amino and hydroxy groups and the electron-deficient carbon atom of CO_2 are demonstrated to lift the degeneracy of the doubly degenerate intramolecular CO_2-bending fundamental significantly with characteristic observed spectral splittings for the amine··CO_2 (≈35–45 cm^{-1}) and alcohol··CO_2 (≈20–25 cm^{-1}) interactions, respectively, despite the almost identically predicted total association energies (≈12–14 $kJ{\cdot}mol^{-1}$) for these van der Waals contacts, as revealed by benchmark Domain-based Local Pair Natural Orbital Coupled Cluster DLPNO-CCSD(T) theory. These high-level theoretical predictions reveal significantly higher "geometry preparation energies" for the amine··CO_2 systems leading to a more severe distortion of the CO_2 linearity upon complexation in agreement with the infrared spectroscopic findings. The systematic combined spectroscopic and quantum chemical evidences for cross-association between CO_2 and amines/alcohols in the present work unambiguously confirm an intriguing binding preference of CO_2 to the hydroxy group of the important carbon capture agent MEA, with an accurate vibrational zero-point energy corrected association energy (D_0) of 13.5 $kJ{\cdot}mol^{-1}$ at the benchmark DLPNO-CCSD(T)/aug-cc-pV5Z level of theory.

Keywords: carbon capture; CO_2; monoethanolamine (MEA); amines; alcohols; vibrational spectroscopy; neon matrices; molecular association; non-covalent interactions; DLPNO-CCSD(T); local energy decomposition

Citation: Hafizi Yazdabadi, S.; Mihrin, D.; Feilberg, K.L.; Wugt Larsen, R. Spectroscopic and Quantum Chemical Evidence of Amine–CO_2 and Alcohol–CO_2 Interactions: Confirming an Intriguing Affinity of CO_2 to Monoethanolamine (MEA). *Molecules* **2024**, *29*, 5521. https://doi.org/10.3390/molecules29235521

Academic Editors: Andrew Clayton and Feng Wang

Received: 30 October 2024
Revised: 14 November 2024
Accepted: 19 November 2024
Published: 22 November 2024

1. Introduction

The concentration of CO_2 in the atmosphere, now exceeding 400 parts per million (ppm), poses a significant challenge as a potent greenhouse gas contributing to global warming and climate change [1]. This rise in CO_2 levels is primarily driven by human activities such as fossil fuel combustion, deforestation, and industrial processes. Despite global efforts to reduce CO_2 emissions through renewable energy adoption, energy efficiency improvements, and policy measures, it has become increasingly clear that mitigation strategies alone are insufficient to address this challenge. Consequently, carbon capture and storage technologies have emerged as an important complementary strategy in the efforts against climate change, aiming to directly remove CO_2 from the atmosphere or prevent its release directly from large-scale industrial sources.

The use of advanced solvents for carbon capture, including biphasic solvents and ionic liquids, has been reported extensively in the literature. Both classes of solvents pro-

vide unique advantages in terms of CO_2 absorption and regeneration efficiency. Biphasic solvents, in particular, are promising due to their phase separation properties at elevated temperatures, potentially lowering the energy demands of CO_2 regeneration compared to traditional aqueous amines [2,3]. Ionic liquids (ILs) have also emerged as promising candidates for CO_2 capture due to their high CO_2 solubility and unique properties, including negligible vapour pressure and recyclability, which qualify them as green solvents. ILs can be customised by modifying their anions or cations, allowing specific tuning of their CO_2 capture capabilities. Various IL types, such as conventional imidazolium-based ILs, task-specific ILs with amino groups, and amino acid-based ILs, have been explored for enhanced CO_2 absorption efficiency [4–10]. For post-combustion CO_2 capture, several non-amine compounds have so far been studied, such as potassium-based and calcium oxide-based sorbents, biochars, and metal–organic materials [11–15].

Despite these alternatives, CO_2 capture research predominantly focuses on amine-based technologies due to their ability to react reversibly and their cost-efficiency with CO_2 [11]. Although some amines such as piperazine have been studied as potential CO_2 absorbing compounds [16–18], the non-volatile alkanolamines containing both a hydroxy and an amino group such as monoethanolamine (MEA) and diethanolamine (DEA), are widely employed as absorbents in CO_2 capture processes [19–22]. A blend of different alkanolamines, such as a combination of a primary (MEA) or secondary (DEA) amine with a tertiary amine, e.g., *N*-methyldiethanolamine (MDEA) leverages the strengths of each. Tertiary amines provide relatively higher CO_2 absorption capacity, while primary and secondary amines offer faster CO_2 reaction rates. The blend improves both the CO_2 absorption efficiency and rate, as well as reducing the energy costs for solvent regeneration in the gas treatment [23,24].

Amine gas treating, also known as amine scrubbing, is a technology where the flue gas is passed through an aqueous amine solution, in which the amine absorbs CO_2 [11,25,26]. It is predicted that by 2030, this method will dominate CO_2 capture technology in coal-fired power plants [26]. Among the various agents employed for CO_2 capture in amine scrubbing and other technologies, monoethanolamine (MEA) stands out as the most widely utilised alkanolamine due to its high reactivity and efficiency in capturing CO_2 from industrial emissions [11,27].

The reaction mechanism of MEA with CO_2 has been a major topic of many investigations [28]. The formation of zwitterion as an intermediate in the carbamate-producing reaction between MEA and CO_2 in aqueous solutions has been investigated with quantum chemical and molecular dynamic simulation in several studies [29–31]. However, a ^{13}C nuclear magnetic resonance study on analyzing the reaction intermediates has shown that the mechanisms of capturing CO_2 in MEA solutions vary with the CO_2 loading [32]. Moreover, the conformations of MEA and the zwitterion intermediate appear to play a crucial role in the reaction pathway. For instance, it has been shown that if the acidic hydrogen in the amino group of a zwitterion forms an intramolecular hydrogen bond with the oxygen in the hydroxy group, rather than interacting with nearby water molecules, CO_2 desorption is more favourable than the deprotonation process [33].

A recent broadband rotational spectroscopic work concerned with the vital cross-association mechanisms of CO_2 with MEA in molecular beams has investigated the initial stages of the gas-phase nucleation between CO_2 and MEA with the aid of extensive systematic theoretical conformational sampling [34]. The sub-nanometer-scale aggregation mechanisms involving the complexation of up to four CO_2 molecules with one MEA molecule under jet-cooled conditions were identified. The subtle competition between the strained directional intramolecular OH$\cdots$N hydrogen bond within MEA and the intermolecular non-directional long-range van der Waals forces associated with the step-wise complexation of CO_2 was uncovered, revealing an intriguing affinity of the first CO_2 molecule to the hydroxy group instead of the amino group. These surprising findings are in contrast to the general understanding of the association between MEA and CO_2 in aqueous solutions [30–33,35,36] and have triggered the present systematic vibrational spectroscopic

exploration of prototypical binary 1:1 weakly bound amine··CO_2 and alcohol··CO_2 van der Waals complexes.

Although weak van der Waals forces usually solely give rise to minor complexation spectral shifts of intramolecular vibrational fundamentals, the aim has been to obtain spectroscopic evidence for the vibrational motion of the engaged functional groups aided by high-level quantum chemical modelling. The vibrational spectral signatures of weakly bound van der Waals complexes are normally only within reach experimentally under jet-cooled conditions in very specific and narrow spectral regions covered by sensitive laser spectroscopy approaches [37–40] but are still achievable with direct absorption in inert doped "quantum matrices" of neon with minor influence of the environment [41] by means of broadband Fourier transform infrared spectroscopy [42–45] at higher optical densities. The present work demonstrates that among the various potential infrared spectroscopic probes for the association between CO_2 and alcohols/amines, the lifting of the doubly degenerate bending transition of CO_2 upon complexation into two components with characteristic observed spectral splittings ≈ 20–45 cm^{-1} (≈3–7%) is a very prominent specific signature for these complexation mechanisms.

2. Results and Discussion

2.1. Infrared Spectrum for the Weakly Bound Binary 1:1 MEA··CO_2 van der Waals Complex

Figure 1 shows the mid-infrared absorption spectra collected for an MEA/CO_2 mixture embedded in neon at 4.2 K in the relevant spectral regions together with a reference spectrum of pure MEA. The inspection of the complete spectral range has enabled the assignments of new emerging vibrational transitions in the spectral intervals revealing the IR-active fundamental transitions associated with the O-H stretching and large-amplitude OH torsional motion of MEA and the bending motion of CO_2. The strongly IR-active OH stretching fundamental, assigned to the binary 1:1 MEA··CO_2 van der Waals complex embedded in neon, is observed at 3538 cm^{-1} and is only slightly red-shifted by 16 cm^{-1} (0.4%) relative to the respective transition for the free MEA monomer reported at 3554 cm^{-1} [46]. A much more significant manifestation of the molecular association is observed for the large-amplitude OH torsional motion of MEA, where this fundamental for the MEA··CO_2 complex is assigned in the far-infrared part of the spectrum at 500 cm^{-1}. This OH torsional fundamental is thereby spectrally blue-shifted by 28 cm^{-1} (6%) relative to the fundamental transition of the free MEA monomer embedded in neon, reported at 472 cm^{-1} previously [46]. The collected spectra do not reveal any new vibrational bands in the vicinity of the previously reported IR-active transitions associated with the asymmetric N-H stretching (3439 cm^{-1}), NH_2 bending (1628 cm^{-1}), and NH_2 wagging (903 cm^{-1}) motions of MEA.

These experimental findings provide the first clue that the CO_2 subunit is not interacting strongly with the amino group, but rather with the hydroxy group of MEA in the cryogenic neon host, as will be supported further when considering the splitting of the doubly degenerate bending fundamental transition of the CO_2 molecule upon complexation. The double degeneracy of this strongly IR-active CO_2 bending fundamental is lifted significantly in the binary 1:1 MEA··CO_2 van der Waals complex resulting in a slightly blue-shifted (by 5 cm^{-1}) transition at 673 cm^{-1} associated with the out-of-plane motion and a more significantly red-shifted (by 18 cm^{-1}) transition at 650 cm^{-1} associated with in-plane motion with respect to the lone pair-donating atom of MEA. The observed splitting of the CO_2-bending fundamental in the order of 23 cm^{-1} (3.5%) relative to the fundamental at 668 cm^{-1} reported for free CO_2 molecules embedded in neon [45] turns out to be a specifically valuable and easily accessible spectroscopic probe for the cross-association mechanisms of CO_2 with amines and alcohols.

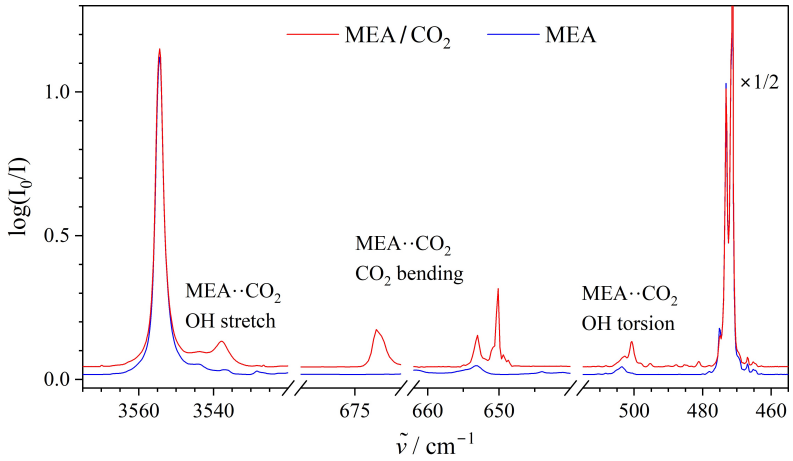

Figure 1. The mid- and far-infrared absorption spectra collected for a MEA/CO_2 mixture (red trace) and pure MEA (blue trace) embedded in neon at 4.2 K for selected spectral intervals with observed fundamental transitions associated with O-H stretching, CO_2 bending and large-amplitude OH torsional motion together with proposed vibrational assignments given for the binary 1:1 MEA·· CO_2 van der Waals complex.

2.2. Infrared Spectra for Weakly Bound Binary 1:1 Amine··CO_2 and Alcohol··CO_2 van der Waals Complexes

Figure 2 shows the series of mid-infrared absorption spectra collected for selected amine/CO_2 and alcohol/CO_2 mixtures embedded in neon at 4.2 K in the relevant spectral region associated with the CO_2-bending fundamental transition together with the spectrum collected for the MEA/CO_2 mixture as a reference. The narrow spectral region of the strongly saturated absorption from the double degenerate bending transition of free monomeric CO_2 at 668 cm^{-1} and the weak absorptions of $(CO_2)_2$ at 670 and 665 cm^{-1} [45], respectively, have been omitted, whereas the absorption from the monomeric bending transition of natural abundant $^{13}CO_2$ at 649 cm^{-1} is observed in all the spectra.

It is evident from inspection of the entire series of spectra that the complexation of CO_2 with both amine and alcohol compounds systematically is manifested as a lifting of the doubly degenerate bending fundamental of the free monomer into two different bending transitions associated with the out-of-plane motion (the narrow 672–674 cm^{-1} spectral range) and in-plane motion (the more extended 632–651 cm^{-1} spectral range) with respect to the lone pair-donating atom of the complexation partner. The spectral signature observed for the weakly bound 1:1 binary ethylamine (EA)··CO_2 van der Waals complex is somewhat broad with a distinct sub-band structure assigned to at least three different conformations of the complex with zero-point corrected dissociation energies within 0.7 kJ·mol^{-1} based on the initial CREST conformational analysis, further RI-MP2 optimisations and single-point energies with the benchmark DLPNO-CCSD(T)/aug-cc-pV5Z methodology (Figure S1c–e in Supporting Information). Theoretical predictions employing the same step-wise procedure for the weakly bound 1:1 binary ethanol (EtOH)··CO_2 van der Waals complex also reveal spectral signatures for two different conformations where the ethanol subunit exists in either the *gauche* or the *trans* conformation (Figure S2b,c) with slightly different band origins for the in-plane CO_2 bending component (653 cm^{-1} and 654 cm^{-1}, respectively, Table 1). The overall trend observed for these spectral signatures of binary 1:1 complexes of CO_2 with the simplest alcohols methanol (MeOH) and ethanol (EtOH) and the simplest alkylated amines methylamine (MA) and ethylamine (EA) is, however, surprisingly convincing, although the CO_2-bending fundamentals only provide indirect information about the exact nature of the binding motifs. The out-of-plane CO_2 bending component turns out to be robustly spectrally blue-shifted by 6–8 cm^{-1} for the entire selection of investigated complexation partners, but interestingly the absolute spectral red-shift of the corresponding in-plane CO_2 bending component specifically appears to depend more delicately on the chemical nature of the complexation partner. The absolute

transition energies for these in-plane CO_2 bending components assigned for the simplest amine··CO_2 van der Waals complexes (640–641 cm^{-1}) are significantly lower than those observed for the corresponding prototypical alcohol··CO_2 van der Waals complexes with band origins in the 653–654 cm^{-1} spectral range. These spectroscopic findings provide empirical evidence that the affinity of the CO_2 molecule to the hydroxy group of MEA is also strongly favoured under inert neon embedding as the observed in-plane CO_2 bending transition for the MEA··CO_2 complex is assigned at 650 cm^{-1}, close to the findings for the simplest alcohol··CO_2 complexes.

Table 1. The observed ($\tilde{\nu}_{exp}$) and predicted harmonic ($\tilde{\omega}$) band origins (cm^{-1}) of the in-plane (ip) and out-of-plane (oop) components of the CO_2 bending transition, the observed ($\Delta\tilde{\nu}_{exp}$) and predicted ($\Delta\tilde{\omega}$) spectral splitting (cm^{-1}) of the doubly degenerate CO_2 bending transition, the "geometry preparation energy" $\Delta E_{geo}(CO_2)$ ($kJ{\cdot}mol^{-1}$) together with the induced distortion angle ($\angle_{distort}$) away from linearity of the CO_2 molecule at equilibrium (180°–theoretically predicted O=C=O angle at equilibrium) upon complexation for the present series of binary 1:1 van der Waals complexes. The structural and harmonic vibrational predictions are computed employing the RI-MP2/aug-cc-pVQZ approach and the "geometry preparation energies" are computed employing the DLPNO-CCSD(T)/aug-cc-pV5Z level of theory.

System	$\tilde{\nu}_{ip}$	$\tilde{\nu}_{oop}$	$\Delta\tilde{\nu}_{exp}$	$\tilde{\omega}_{ip}$	$\tilde{\omega}_{oop}$	$\Delta\tilde{\omega}$	$\Delta E_{geo}(CO_2)$	$\angle_{distort}$
Methanol··CO_2	654	672	18	651	668	17	0.31	2.10
Ethanol··CO_2 (*g*)	653	672	19	643	669	26	0.35	2.16
Ethanol··CO_2 (*t*)	653	672	19	648	667	19	0.25	1.95
Monoethanolamine··CO_2	650	673	23	643	668	25	0.47	2.49
Methylamine··CO_2	641	674	33 [47]	633	677	44	0.67	2.94
Ethylamine··CO_2	640	673	33	632	675	43	0.71	2.98
Dimethylamine··CO_2	634	673	39	626	669	43	0.93	3.42
Trimethylamine··CO_2	627	673	46	612	670	58	1.27	3.99

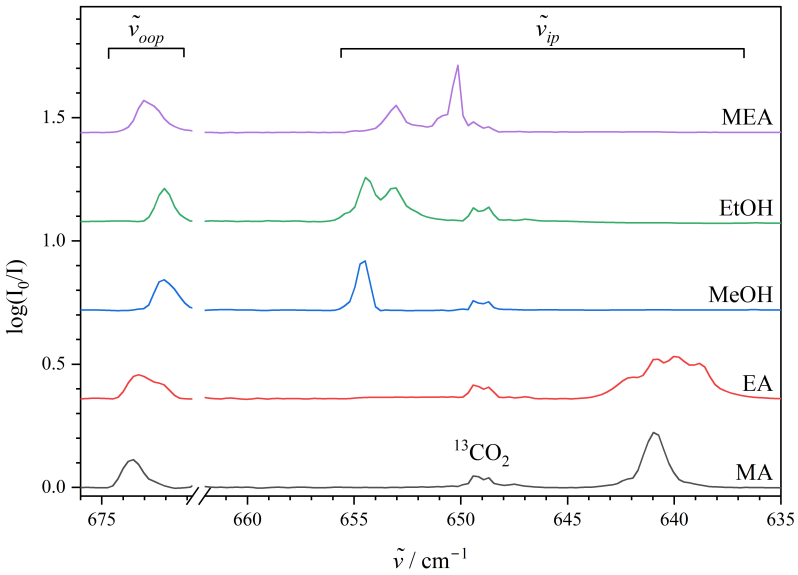

Figure 2. The infrared absorption spectra in the CO_2-bending region (635–680 cm^{-1}) collected for neon "quantum matrices" at 4.2 K doped with mixtures of CO_2 and methylamine, ethylamine, methanol, and ethanol, and monoethanolamine. The assignments of the red-shifted in-plane ($\tilde{\nu}_{ip}$) and blue-shifted out-of-plane ($\tilde{\nu}_{oop}$) components of the CO_2-bending transition for the binary weakly bound 1:1 van der Waals complexes are indicated together with the absorption from the monomeric bending transition of natural abundant $^{13}CO_2$ at 649 cm^{-1} [45]. The narrow region of the strongly saturated absorption from the bending transition of regular monomeric CO_2 at 668 cm^{-1} [45] has been omitted for clarity.

Before consulting the predictions from theoretical conformational analyses and refined high-level ab initio computations, the pronounced lifting of the degenerate CO_2-bending fundamental upon the association with amines has been explored further experimentally for an extended set including both ammonia and more alkylated amine compounds. Figure 3 shows the infrared absorption spectra collected for ammonia/CO_2, methylamine (MA)/CO_2, dimethylamine (DMA)/CO_2 and trimethylamine (TMA)/CO_2 mixtures embedded in neon at 4.2 K in the relevant spectral region associated with the CO_2-bending fundamental transition. This extended spectral series confirms that the slightly spectrally blue-shifted out-of-plane CO_2 bending component is basically unaffected by the specific amine complexation partner and is also observed at 673 cm^{-1} for both the binary 1:1 ammonia··CO_2 and trimethylamine (TMA)··CO_2 van der Waals complexes. The spectrally red-shifted in-plane CO_2 bending component of the latter (TMA)··CO_2 system involving a tertiary amine reveals some sub-band structures indicating multiple conformations of the complex although the dominating transition for the most favoured conformation is easily assigned at 627 cm^{-1}. This witnesses the largest splitting of 46 cm^{-1} (6.9%) observed for the degenerate CO_2 bending fundamental of the entire set of investigated complexation partners (Table 1). The complexation of CO_2 with the secondary amine, DMA, reveals a less spectrally red-shifted in-plane CO_2 bending component at 634 cm^{-1} for the most stable conformation, whereas the association with the simplest amine, ammonia, reveals the corresponding transition at 648 cm^{-1} and thereby almost in the vicinity of the observations for the set of alcohol··CO_2 van der Waals complexes. It is interesting to note that the observed spectral splitting of the degenerate CO_2-bending fundamental consequently increases almost linearly with the number of methyl groups replacing H atoms on the ammonia molecule in the series of primary, secondary, and tertiary amines as complexation partners (TMA··CO_2 > DMA··CO_2 > MA··CO_2 [47] > ammonia··CO_2). This observation perfectly correlates with the linear change in the gas-phase basicity of amines with the increase of alkyl substitution, which has been explained by the increase in the polarisability of the molecule [48,49]. These observations will be supported further by the present exploratory quantum chemical predictions.

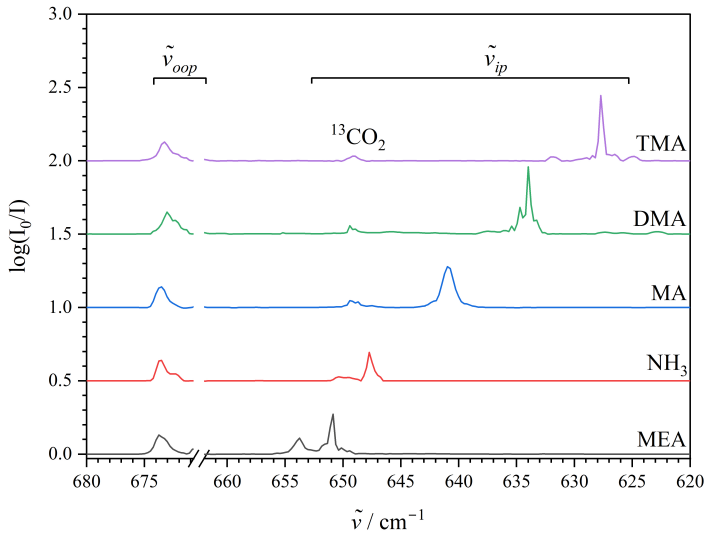

Figure 3. The infrared absorption spectra in the CO_2-bending region (620–680 cm^{-1}) collected for neon "quantum matrices" at 4.2 K doped with mixtures of CO_2 with monoethanolamine (MEA), ammonia, methylamine (MA), dimethylamine (DMA), and trimethylamine (TMA). The assignments of the red-shifted in-plane ($\tilde{\nu}_{ip}$) and blue-shifted out-of-plane ($\tilde{\nu}_{oop}$) components of the CO_2 bending transition for the binary weakly bound 1:1 van der Waals complexes are indicated together with the absorption from the monomeric bending transition of natural abundant $^{13}CO_2$ at 649 cm^{-1} [45]. The narrow region of the strongly saturated absorption from the bending transition of regular monomeric CO_2 at 668 cm^{-1} [45] has been omitted for clarity.

2.3. Quantum Chemical Conformational Analysis of the Weakly Bound Binary 1:1 Amine··CO_2 and Alcohol··CO_2 van der Waals Complexes

The global potential energy minimum geometry of the weakly bound binary 1:1 MEA··CO_2 van der Waals complex identified via the CREST conformational space exploration tool by Schnell et al. [34], further optimised initially by the B3LYP-D4/aug-cc-pVQZ approach and subsequently employing the RI-MP2/aug-cc-pVQZ methodology, is visualised in Figure 4. In this global minimum structure the intramolecular O–H· · · N hydrogen bond of MEA persist and the C atom of the CO_2 subunit has established a van der Waals contact with the O atom on the hydrogen bond donating OH group. The refined DLPNO-CCSD(T)/aug-cc-pV5Z electronic energy corrections in combination with the RI-MP2/aug-cc-pVQZ harmonic vibrational zero-point energy corrections provides a dissociation energy D_0 13.5 kJ·mol^{-1}.

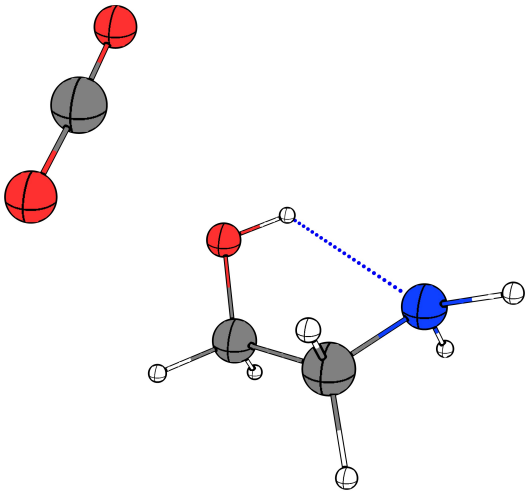

Figure 4. The most stable conformation for the binary MEA··CO_2 van der Waals complex as reported in Ref. [34] and re-optimised at the RI-MP2/aug-cc-pVQZ level of theory.

Table 2 shows the harmonically predicted complexation spectral shifts ($\Delta\omega = \omega_{complex} - \omega_{monomer}$) for the most IR-active O-H stretching, OH torsional, asymmetric NH_2 stretching, NH_2 bending and NH_2 wagging fundamentals together with the predicted splitting of the degenerate CO_2 bending fundamental for the MEA··CO_2 van der Waals complex. It is evident that the present observations are strongly supported even by these harmonic vibrational computations at the RI-MP2/aug-cc-pVQZ level of theory. This calculation predicts a harmonic spectral red-shift of 20 cm^{-1} owing to a minor predicted elongation of the O-H bond of 0.001 Å upon complexation (relative to the experimental spectral red-shift of 16 cm^{-1}) and accordingly the harmonic calculation predicts a spectral blue-shift of 24 cm^{-1} for the OH torsional fundamental (relative to the experimental spectral blue-shift of 28 cm^{-1}) resulting from a slightly stabilisation of the intramolecular O–H· · · N hydrogen bond within the MEA molecule upon complexation with CO_2 (shortening by 0.02 Å). The agreement between experiment and this harmonic prediction is surprisingly good considering the expected extent of anharmonic character for the latter large-amplitude torsional motion. The fact that the present experimental work does not allow any unambiguous assignments for the perturbed IR-active asymmetric NH_2 stretching, NH_2 bending and NH_2 wagging fundamentals of the binary MEA··CO_2 complex indirectly supports that the global potential energy minimum predicted and observed by Schnell et al. in molecular beams is also observed in the cryogenic neon "quantum matrix" environment. According to the harmonic vibrational predictions for this most stable conformation, all the spectral shifts of these fundamentals upon complexation should be less than 1 cm^{-1} and thus negligible. Interestingly, the experimentally observed splitting of the CO_2 bending fundamental of 23 cm^{-1} is also in excellent agreement with the harmonic prediction of 25 cm^{-1} and thereby significant less than observed for the investigated series of amine··CO_2 van der Waals com-

plexes. The animations of the two predicted (in-plane and out-of-plane) components of the motion associated with the CO_2 bending fundamental introduced with the complexation are visualised in Figure 5. The unexpected observed dependence of this spectral splitting on the exact intermolecular van der Waals binding motif is explored further by the exploratory theoretical predictions for the entire set of van der Waals complexes.

Table 2. Experimental ($\tilde{\nu}_{exp}$) and RI-MP2/aug-cc-pVQZ predicted harmonic ($\tilde{\omega}$) band origins (intensities given in parentheses, units of km·mol^{-1}) for vibrational fundamental transitions associated with the IR-active O-H stretching, OH torsional, asymmetric NH_2 stretching, NH_2 bending and NH_2 wagging fundamentals together with the two components of the CO_2 bending fundamental of the MEA··CO_2 van der Waals complex together with the observed complexation shifts $\Delta\tilde{\nu}_{exp}$ and the harmonically predicted complexation shifts $\Delta\tilde{\omega}$ (units of cm^{-1}).

Mode Description	System	$\tilde{\omega}$	$\Delta\tilde{\omega}$	$\tilde{\nu}_{exp}$	$\Delta\tilde{\nu}_{exp}$
OH str	MEA	3748 (76)		3554 [46]	
	MEA··CO_2	3728 (88)	−20	3538	−16
NH_2 asym str	MEA	3640 (10)		3439 [46]	
	MEA··CO_2	3641 (11)	1	-	-
NH_2 bend	MEA	1652 (30)		1628	
	MEA··CO_2	1652 (30)	0	-	-
NH_2 wag	MEA	932 (45)		903	
	MEA··CO_2	931 (48)	−1	-	-
OH tors	MEA	557 (89)		472 [46]	
	MEA··CO_2	581 (95)	24	500	28
CO_2 bend	CO_2	664 (23)		668 [45]	
	MEA··CO_2 ip	643 (52)	−21	650	−18
	MEA··CO_2 oop	668 (26)	4	673	5

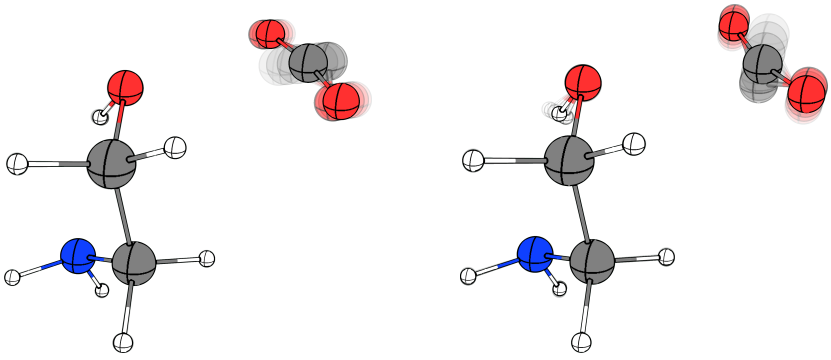

(**a**) In-plane CO_2 bending (**b**) Out-of-plane CO_2 bending

Figure 5. Visualisation of the two components of the CO_2-bending fundamental for the most stable conformation of the binary 1:1 MEA··CO_2 van der Waals complex. (**a**) in-line with the lone pair-donating atom (in-plane, red-shifted from CO_2 monomer) experimentally observed at 650 cm^{-1} (**b**) perpendicular (out-of-plane, blue-shifted from CO_2 monomer) experimentally observed at 673 cm^{-1}.

Table 1 shows the two harmonically predicted components of the CO_2-bending fundamental for the investigated series of weakly bound van der Waals complexes. In general, the predicted spectral splittings slightly overestimate the experimental values except for the methanol··CO_2 system, where the smallest observed splitting (18 cm^{-1}) is slightly larger than the theoretical (17 cm^{-1}) predictions. The theoretical predictions ($\Delta\tilde{\omega}$) strongly support the experimental findings ($\Delta\tilde{\nu}_{exp}$) that the splitting of the two different classes of alcohol··CO_2 and amine··CO_2 van der Waals complexes falls into two categories; $\Delta\tilde{\nu}_{exp}$ $\approx$ 20 cm^{-1} and $\Delta\tilde{\omega} \approx$ 20–25 cm^{-1} for the alcohol··CO_2 systems and $\Delta\tilde{\nu}_{exp} \approx$ 35–45 cm^{-1} and $\Delta\tilde{\omega} \approx$ 45–55 cm^{-1} for the amine··CO_2 systems. The splitting of the latter class of systems, however, seems to be more prone to the exact nature of the alkyl substituents.

This lifting of the doubly degeneracy of the CO_2-bending fundamental upon complexation is due to a distortion of the molecule's linear equilibrium structure as supported by the optimised "distortion angles" and the predicted "geometry preparation energies" for the investigated series of complexes given in Table 1. The distortion angle $\angle_{distort}$, defined as the difference between the predicted equilibrium O=C=O angle in a specific complex relative to the equilibrium O=C=O angle of 180° for the free non-bonded CO_2 molecule, is shown to increase significantly when CO_2 interacts with an amino group relative to the situation when a CO_2 interacts with a hydroxy group for molecules with the same alkyl substituents although the total predicted interaction energies D_0 are almost identical for the two different classes of 1:1 van der Waals complexes (Table 3). The O=C=O angle is distorted by 1.95–2.16° for the investigated alcohol··CO_2 systems upon complexation, whereas this angle is distorted by 2.94–3.99° for the amine··CO_2 systems. The distortion of the O=C=O angle in the most stable conformation of the MEA··CO_2 van der Waals complex is predicted to be 2.49°, which is only slightly more than for the corresponding alcohol··CO_2 series (but significantly less than for the amine··CO_2 series) owing to the additional polarisation of the hydroxy group engaging in the intramolecular O–H· · · N hydrogen bond with the amino group of MEA. The same trend is mirrored in the computed values of the "geometry preparation energy" for the CO_2 subunit, given for each of the investigated binary van der Waals complexes in Table 1, providing an estimate of the energy "cost" when the CO_2 subunit is distorted upon complexation. These computed geometry preparation energies show that the the attractive stabilising forces in general are still slightly stronger for the van der Waals contacts between CO_2 and amino groups than between the CO_2 and hydroxy groups, although the total theoretical association energies are almost identical at the benchmark DLPNO-CCSD(T)/aug-cc-pV5Z level of theory. The geometry preparation energies are for example computed to 0.31 and 0.67 kJ·mol^{-1} for the methanol··CO_2 and the methylamine··CO_2 systems where the total zero-point corrected dissociation energies D_0 are calculated to 12.1 and 11.9 kJ·mol^{-1}, respectively. The same trend is observed for the pair of ethanol··CO_2 and ethylamine··CO_2 van der Waals complexes of similar size when considering both the computed geometry preparation energies and total zero-point corrected dissociation energies.

Table 3. Electronic energies D_e, harmonic vibrational zero-point energy factors ΔZPE and resulting corrected dissociation energies D_0 for the investigated binary alcohol··CO_2 and amine··CO_2 van der Waals complexes optimised at the B3LYP-D4/aug-cc-pVQZ and RI-MP2/aug-cc-pVQZ levels together with single-point electronic energies at the DLPNO-CCSD(T)/aug-cc-pV5Z level (units of kJ·mol^{-1}).

	B3LYP-D4			**RI-MP2**			**DLPNO-CCSD(T)**	
System	D_e	**ΔZPE**	D_0	D_e	**ΔZPE**	D_0	D_e [1]	D_0 [2]
Methanol··CO_2	14.3	2.7	11.5	15.1	2.8	12.3	14.9	12.1
Ethanol··CO_2 (*t*)	14.0	2.2	11.8	15.2	2.2	13.0	14.9	12.7
Ethanol··CO_2 (*g*)	14.3	2.5	11.8	15.1	2.4	12.7	14.8	12.5
Monoethanolamine··CO_2	15.5	2.6	12.9	16.8	2.5	14.3	16.0	13.5
Methylamine··CO_2	15.2	2.9	12.4	15.4	3.0	12.4	14.9	11.9
Ethylamine··CO_2	16.0	2.8	13.2	16.8	3.0	13.8	15.9	12.9
DMA	16.8	2.7	14.1	18.1	2.7	15.4	16.6	14.0
TMA	18.0	2.6	15.4	20.1	2.2	17.9	17.9	15.7

[1] Electronic dissociation energies calculated at the DLPNO-CCSD(T)/aug-cc-pV5Z level based on optimised geometries at the RI-MP2/aug-cc-pVQZ level. [2] Based on D_e-values at the DLPNO-CCSD(T)/aug-cc-pV5Z level in combination with ΔZPE-values at the RI-MP2/aug-cc-pVQZ level.

3. Materials and Methods

3.1. Experimental Details

The experimental facility consists of a Bruker Vertex 80V Fourier-transform spectrometer (Ettlingen, Germany) in combination with a customised 4 K closed-cycle cryo-cooler

(Model DE-204, Advanced Research Systems, Inc., Macungie, PA, USA). A direct transmission oxygen-free high-conductivity copper window holder attached with a wedged diamond sample window (Diamond Materials, GmbH, Freiburg im Breisgau, Germany) has been mounted onto the cold head of the cryo-cooler [50]. The cryostat is surrounded by a rotatable vacuum shroud equipped with two additional wedged diamond windows together with a gate valve allowing the insertion of the inlet copper tubes into the vacuum space of the cryostat [51]. The wedged diamond windows minimise spectral interference fringes from internal reflections in the windows. The optical arrangement of the spectrometer consists of an air-cooled Globar thermal radiation source, a Ge-coated KBr beam splitter together with a broad-band LN_2-cooled HgCdTe detector for the complete infrared spectral range (450–4500 cm^{-1}). A spectral resolution of 0.6 cm^{-1} has been applied throughout the measurements as the best compromise between the resulting signal-to-noise ratio and sufficient spectral resolution to resolve the observed vibrational sub-band structures.

The doped neon "quantum matrices" are obtained by the simultaneous deposition of neon gas (99.999%, Air Liquide Danmark A/S, Taastrup, Denmark) and co-deposition of specific samples through separate inlet tubes, which are brought to within 5 mm of the cold sample diamond window employing a motorised stage [52]. The neon gas is supplied from a mass flow controller (G-series, MKS Instruments, Inc., Andover, MA, USA) at a flow rate of 6–8 sccm depending on the desired mixing ratio and pre-cooled with a LN_2-cooled trap (77 K). Methanol (99.9%, Sigma Aldrich, Søborg, Denmark) and ethanol (99.9%, Sigma Aldrich, Søborg, Denmark) vapours were premixed with CO_2 (99.999%, AGA A/S, Ballerup, Denmark) beforehand, while the samples of the selected amines and CO_2 were co-deposited separately and flow regulated with fine metering valves. The samples of amines including ammonia (25 wt.%, AnalaR NORMAPUR, VWR Int., Søborg, Denmark), methylamine (40 wt.%, Sigma Aldrich, Søborg, Denmark), ethylamine (66.0–72.0 wt.%, Sigma Aldrich, Søborg, Denmark), dimethylamine (40 wt.%, Sigma Aldrich, Søborg, Denmark) and trimethylamine (25 wt.%, Sigma Aldrich, Søborg, Denmark) were all extracted from the aqueous solutions under vacuum. Pumped and pre-baked molecular sieves (4 Å) have been employed to reduce minor traces of H_2O in the non-volatile MEA sample (99%, Sigma Aldrich, Søborg, Denmark) while depositing MEA directly from a sublimation vessel thermostated to −7 °C [46]. The combined deposition procedures of neon host and the alcohol/CO_2 and amine/CO_2 sample mixtures onto the wedged diamond window were carried out simultaneously for a period of two hours.

Following the acquisition of the initial pre-annealing spectra, the neon "quantum matrices" were gently annealed by raising the temperature to 9.5 K for 60 min. The temperature is regulated by a combination of resistive heaters and silicon diode temperature sensors attached to the window holder and feedback electronics operated by a PID temperature controller (Model 335, LakeShore, Westerville, OH, USA). Subsequently, the heater was deactivated, allowing the sample temperature to relax back to 4–5 K before the collection of post-annealing spectra. The annealing softens the solid neon environment and usually circumvents rare residual matrix site splittings [53,54]. This procedure furthermore triggers the diffusion of molecules within the matrix accelerating the cross-association of CO_2 and the co-deposited alcohol/amine samples into weakly bound van der Waals cluster molecules. The background spectra were all collected of the fully evacuated cryostat at room temperature at the end of the experiments.

3.2. Computational Details

Quantum chemical calculations were performed using the Conformer-Rotamer Ensemble Sampling Tool CREST (version 2.12, Bonn, Germany) [55] and the ORCA quantum chemistry program package (version 5.0.4, Max-Planck-Institut für Kohlenforschung, Mülheim an der Ruhr, Germany) [56–58], both installed on the DTU High-Performance Computing (HPC) cluster [59]. The CREST tool with the NCI mode and the GFN2-xTB methodology [60] was employed to generate the most stable conformations of the investigated binary 1:1 alcohol–CO_2 and amine–CO_2 van der Waals complexes. For each

system, the first 10–15 conformations identified by the CREST utility were selected for further optimisations. These conformations underwent further geometry optimisation and harmonic vibrational frequency calculations using the dispersion-corrected B3LYP-D4 methodology [61–63], in combination with the aug-cc-pVQZ basis set and the RIJ-COSX approximation [64–66].

Following the B3LYP-D4 optimisation step, further geometry optimisations and harmonic vibrational frequency calculations were repeated using the RI-MP2 methodology [67–69], employing the same basis sets and approximations as for the B3LYP-D4 calculations. Finally, the optimised potential energy minima geometries obtained from the RI-MP2 calculations were employed for single-point energy calculations with Domain-based Local Pair Natural Orbital Coupled Cluster with Single, Double, and Perturbative Triple excitations (DLPNO-CCSD(T)) [70–74]. This step involved the aug-cc-pV5Z basis set, together with the RI-JK approximation [75] and tight PNO screening criteria [76] to provide the electronic dissociation energies (D_e) and vibrational zero-point energy corrected dissociation energies (D_0) ensuring highly accurate energy estimations. The geometric distortion of the linear CO_2 fragment caused by intermolecular interaction has been estimated via the "geometry preparation energy", which is calculated as the electronic energy difference between the CO_2 subunit in the distorted geometry as found in the respective van der Waals complex, and the energy of the isolated CO_2 molecule employing the above-described combination of DLPNO-CCSD(T)/RI-MP2 electronic structure methodologies.

4. Conclusions

The present work reports a systematic infrared spectroscopic investigation of a series of weakly bound alcohol–CO_2 and amine–CO_2 van der Waals cluster molecules embedded in inert "quantum" matrices of neon at 4.2 K triggered by the recent broadband rotational spectroscopic investigation of the MEA-CO_2 van der Waals complex in molecular beams [34] revealing (indirectly) an intriguing affinity of CO_2 to the hydroxy group of MEA. The combined vibrational spectroscopic findings and harmonic RI-MP2/aug-cc-pVQZ quantum chemical predictions help to assign both the strongly IR-active vibrational fundamentals associated with the O-H stretching motion at 3538 cm^{-1} (slightly spectrally red-shifted by 16 cm^{-1} (0.4%) relative to the free MEA monomer) and large-amplitude OH torsional motion at 500 cm^{-1} (spectrally blue-shifted by 28 cm^{-1} (6%) relative to the free MEA monomer) of the MEA··CO_2 van der Waals complex. The collected spectra did not reveal any bands in the vicinity of the previously reported IR-active vibrational transitions associated with the asymmetric N-H stretching, NH_2 bending and NH_2 wagging fundamentals of MEA. The present findings reveal that the non-covalent complexation of CO_2 with MEA is manifested as a significant lifting of the doubly degenerate CO_2-bending fundamental of the free molecule into two different components associated with out-of-plane (slightly blue-shifted) and in-plane (significantly red-shifted) bending motion resulting in a spectral splitting of 23 cm^{-1} in accordance with the splitting of 25 cm^{-1} from the harmonic predictions. The out-of-plane CO_2 bending component turns out to be systematically spectrally blue-shifted by 6–8 cm^{-1} for the entire selection of investigated alcohol··CO_2 and amine··CO_2 van der Waals complexes, whereas the absolute spectral red-shift of the corresponding in-plane CO_2 bending component appears to be specifically dependent on the chemical nature of the complexation partner. Our present findings reveal characteristic spectral splittings for the amine··CO_2 (≈35–45 cm^{-1}) and alcohol··CO_2 (≈20–25 cm^{-1}) interactions, respectively, despite the almost identically predicted total association energies (≈12–14 $kJ{\cdot}mol^{-1}$) for these van der Waals contacts as revealed by benchmark domain-based local pair natural orbital coupled cluster DLPNO-CCSD(T) theory. The spectroscopic findings provide unambiguous complementary empirical evidence that the affinity of the CO_2 molecule to the hydroxy group of MEA is also strongly favored in inert neon "quantum matrices".

Supplementary Materials: The following supporting information can be downloaded at: https://www.mdpi.com/article/10.3390/molecules29235521/s1, The material contains the optimized potential energy minima geometries of the studied alcoholes, amines, and monoethanolamine van der waals complex with CO_2 in XYZ format, the visualization of the respective structures and the predicted harmonic vibrational mode frequencies for the MEA/CO_2 complex.

Author Contributions: Conceptualization—R.W.L.; Methodology—D.M. and R.W.L.; Software—S.H.Y. and D.M.; Validation—S.H.Y., D.M. and R.W.L.; Formal analysis—S.H.Y., D.M. and R.W.L.; Investigation—S.H.Y., D.M. and R.W.L.; Resources—K.L.F. and R.W.L.; Data curation—S.H.Y. and R.W.L.; Writing—original draft preparation—S.H.Y. and R.W.L.; Writing—review and editing—S.H.Y., D.M., K.L.F. and R.W.L.; Visualization—S.H.Y.; Supervision—K.L.F. and R.W.L.; Project administration—K.L.F. and R.W.L.; Funding acquisition—K.L.F. and R.W.L. All authors have read and agreed to the published version of the manuscript.

Funding: This research was funded by the Danish Offshore Technology Centre (DTU Offshore).

Institutional Review Board Statement: Not applicable.

Informed Consent Statement: Not applicable.

Data Availability Statement: Data are contained within the article and Supplementary Materials.

Acknowledgments: The authors acknowledge the DTU Computing Center for access to the high-performance computing services and the technical support provided. Finally, Alexandre Voute and the mechanical workshop at DTU Chemistry is acknowledged for help and advice in the design of the experimental facilities.

Conflicts of Interest: The authors declare no conflicts of interest.

References

1. Hashimoto, K. Global Temperature and Atmospheric Carbon Dioxide Concentration. In *Global Carbon Dioxide Recycling*; Springer: Singapore, 2019; pp. 5–17. [CrossRef]
2. Zhang, G.; Qian, J.; Liu, J.; Yu, T.; Liu, Q. Insight and assessment of CO_2 capture using diethylenetriamine/2-(diethylamino)ethanol/n-propanol water-lean biphasic solvent: Experimental and quantum chemical calculation. *Chem. Eng. J.* **2024**, *500*, 156834. [CrossRef]
3. Jin, L.; Hou, X.; Zhan, L.; Hou, D.; Gu, L.; Zhang, D.; Shen, J.; Zheng, Z.; Lv, C.; Liu, S.; et al. Analysis of the changes in the absorption and regeneration performance of diethylenetriamine in carbon capture environments with functionalized alcohols and mixed amines. *Fuel* **2024**, *368*, 131375. [CrossRef]
4. Shaikh, A.R.; Ashraf, M.; AlMayef, T.; Chawla, M.; Poater, A.; Cavallo, L. Amino acid ionic liquids as potential candidates for CO_2 capture: Combined density functional theory and molecular dynamics simulations. *Chem. Phys. Lett.* **2020**, *745*, 137239. [CrossRef]
5. Earle, M.J.; Seddon, K.R. Ionic liquids. Green solvents for the future. *Pure Appl. Chem.* **2000**, *72*, 1391–1398. [CrossRef]
6. Brennecke, J.F.; Maginn, E.J. Ionic liquids: Innovative fluids for chemical processing. *AIChE J.* **2001**, *47*, 2384–2389. [CrossRef]
7. Shim, Y.; Jeong, D.; Manjari, S.; Choi, M.Y.; Kim, H.J. Solvation, Solute Rotation and Vibration Relaxation, and Electron-Transfer Reactions in Room-Temperature Ionic Liquids. *Acc. Chem. Res.* **2007**, *40*, 1130–1137. [CrossRef]
8. Cadena, C.; Anthony, J.L.; Shah, J.K.; Morrow, T.I.; Brennecke, J.F.; Maginn, E.J. Why Is CO_2 So Soluble in Imidazolium-Based Ionic Liquids? *J. Am. Chem. Soc.* **2004**, *126*, 5300–5308. [CrossRef]
9. Bates, E.D.; Mayton, R.D.; Ntai, I.; Davis, J.H. CO_2 Capture by a Task-Specific Ionic Liquid. *J. Am. Chem. Soc.* **2002**, *124*, 926–927. [CrossRef]
10. Bao, W.; Wang, Z.; Li, Y. Synthesis of Chiral Ionic Liquids from Natural Amino Acids. *J. Org. Chem.* **2003**, *68*, 591–593. [CrossRef]
11. Dutcher, B.; Fan, M.; Russell, A.G. Amine-based CO_2 capture technology development from the beginning of 2013—A review. *ACS Appl. Mater. Interfaces* **2015**, *7*, 2137–2148. [CrossRef]
12. Plaza, M.; González, A.; Pis, J.; Rubiera, F.; Pevida, C. Production of microporous biochars by single-step oxidation: Effect of activation conditions on CO_2 capture. *Appl. Energy* **2014**, *114*, 551–562. [CrossRef]
13. Nugent, P.; Giannopoulou, E.G.; Burd, S.D.; Elemento, O.; Forrest, K.; Pham, T.; Ma, S.; Space, B.; Wojtas, L.; Eddaoudi, M.; et al. Porous materials with optimal adsorption thermodynamics and kinetics for CO_2 separation. *Nature* **2013**, *495*, 80–84. [CrossRef]
14. Lee, S.C.; Kwon, Y.M.; Jung, S.Y.; Lee, J.B.; Ryu, C.K.; Kim, J.C. Excellent thermal stability of potassium-based sorbent using ZrO_2 for post combustion CO_2 capture. *Fuel* **2014**, *115*, 97–100. [CrossRef]
15. Sedghkerdar, M.H.; Mahinpey, N.; Sun, Z.; Kaliaguine, S. Novel synthetic sol-gel CaO based pellets using porous mesostructured silica in cyclic CO_2 capture process. *Fuel* **2014**, *127*, 101–108. [CrossRef]

16. Rochelle, G.; Chen, E.; Freeman, S.; Van Wagener, D.; Xu, Q.; Voice, A. Aqueous piperazine as the new standard for CO_2 capture technology. *Chem. Eng. J.* **2011**, *171*, 725–733. [CrossRef]
17. Freeman, S.A.; Dugas, R.; Van Wagener, D.H.; Nguyen, T.; Rochelle, G.T. Carbon dioxide capture with concentrated, aqueous piperazine. *Int. J. Greenh. Gas Control* **2010**, *4*, 119–124. [CrossRef]
18. Chen, X.; Rochelle, G.T. Aqueous piperazine derivatives for CO_2 capture: Accurate screening by a wetted wall column. *Chem. Eng. Res. Des.* **2011**, *89*, 1693–1710. [CrossRef]
19. Yu, C.H.; Huang, C.H.; Tan, C.S. A review of CO_2 capture by absorption and adsorption. *Aerosol Air Qual. Res.* **2012**, *12*, 745–769. [CrossRef]
20. Kubota, Y.; Bučko, T. Carbon dioxide capture in 2,2′-iminodiethanol aqueous solution from ab initio molecular dynamics simulations. *J. Chem. Phys.* **2018**, *149*, 224103. [CrossRef]
21. Narku-Tetteh, J.; Muchan, P.; Idem, R. Effect of alkanol chain length of primary alkanolamines and alkyl chain length of secondary and tertiary alkanolamines on their CO_2 capture activities. *Sep. Purif. Technol.* **2017**, *187*, 453–467. [CrossRef]
22. Jackson, P.; Beste, A.; Attalla, M. Insights into amine-based CO_2 capture: An ab initio self-consistent reaction field investigation. *Struct. Chem.* **2011**, *22*, 537–549. [CrossRef]
23. Narimani, M.; Amjad-Iranagh, S.; Modarress, H. CO_2 absorption into aqueous solutions of monoethanolamine, piperazine and their blends: Quantum mechanics and molecular dynamics studies. *J. Mol. Liq.* **2017**, *233*, 173–183. [CrossRef]
24. Samanta, A.; Bandyopadhyay, S.S. Absorption of carbon dioxide into aqueous solutions of piperazine activated 2-amino-2-methyl-1-propanol. *Chem. Eng. Sci.* **2009**, *64*, 1185–1194. [CrossRef]
25. Rochelle, G. 3—Conventional amine scrubbing for CO_2 capture. In *Absorption-Based Post-Combustion Capture of Carbon Dioxide*; Feron, P.H., Ed.; Woodhead Publishing: Cambridge, UK, 2016; pp. 35–67. [CrossRef]
26. Rochelle, G.T. Amine Scrubbing for CO_2 Capture. *Science* **2009**, *325*, 1652–1654. [CrossRef]
27. Yang, X.; Rees, R.J.; Conway, W.; Puxty, G.; Yang, Q.; Winkler, D.A. Computational Modeling and Simulation of CO_2 Capture by Aqueous Amines. *Chem. Rev.* **2017**, *117*, 9524–9593. [CrossRef]
28. Iida, K.; Sato, H. Proton transfer step in the carbon dioxide capture by monoethanol amine: A theoretical study at the molecular level. *J. Phys. Chem. B* **2012**, *116*, 2244–2248. [CrossRef]
29. Hwang, G.S.; Stowe, H.M.; Paek, E.; Manogaran, D. Reaction mechanisms of aqueous monoethanolamine with carbon dioxide: A combined quantum chemical and molecular dynamics study. *Phys. Chem. Chem. Phys.* **2015**, *17*, 831–839. [CrossRef]
30. Kubota, Y.; Ohnuma, T.; Bučko, T. Carbon dioxide capture in 2-aminoethanol aqueous solution from ab initio molecular dynamics simulations. *J. Chem. Phys.* **2017**, *146*, 094303. [CrossRef]
31. Xie, H.; Wang, P.; He, N.; Yang, X.; Chen, J. Toward rational design of amines for CO_2 capture: Substituent effect on kinetic process for the reaction of monoethanolamine with CO_2. *J. Environ. Sci.* **2015**, *37*, 75–82. [CrossRef]
32. Lv, B.; Guo, B.; Zhou, Z.; Jing, G. Mechanisms of CO_2 Capture into Monoethanolamine Solution with Different CO_2 Loading during the Absorption/Desorption Processes. *Environ. Sci. Technol.* **2015**, *49*, 10728–10735. [CrossRef]
33. Xie, H.B.; Zhou, Y.; Zhang, Y.; Johnson, J.K. Reaction mechanism of monoethanolamine with CO_2 in aqueous solution from molecular modeling. *J. Phys. Chem. A* **2010**, *114*, 11844–11852. [CrossRef]
34. Xie, F.; Sun, W.; Pinacho, P.; Schnell, M. CO_2 Aggregation on Monoethanolamine: Observations from Rotational Spectroscopy. *Angew. Chem.-Int. Ed.* **2023**, *62*, e202218539. [CrossRef]
35. Han, B.; Zhou, C.; Wu, J.; Tempel, D.J.; Cheng, H. Understanding CO_2 Capture Mechanisms in Aqueous Monoethanolamine via First Principles Simulations. *J. Phys. Chem. Lett.* **2011**, *2*, 522–526. [CrossRef]
36. Davran-Candan, T. DFT Modeling of CO_2 Interaction with Various Aqueous Amine Structures. *J. Phys. Chem. A* **2014**, *118*, 4582–4590. [CrossRef]
37. Barclay, A.; McKellar, A.; Moazzen-Ahmadi, N. Infrared spectra of $(CO_2)_2$–Rg trimers, Rg = Ne, Ar, Kr, and Xe. *J. Mol. Spectrosc.* **2022**, *387*, 111673. [CrossRef]
38. Barclay, A.J.; McKellar, A.R.W.; Moazzen-Ahmadi, N. Spectra of CO_2–N_2 dimer in the 4.2 μm region: Symmetry breaking of the intramolecular CO_2 bend, the intermolecular bend, and higher *K*-Values Fundam. *J. Chem. Phys.* **2020**, *153*, 014303. [CrossRef]
39. Oliaee, J.N.; Dehghany, M.; Moazzen-Ahmadi, N.; McKellar, A.R.W. Spectroscopic identification of carbon dioxide clusters: $(CO_2)_6$ to $(CO_2)_{13}$. *Phys. Chem. Chem. Phys.* **2011**, *13*, 1297–1300. [CrossRef]
40. Norooz Oliaee, J.; Dehghany, M.; McKellar, A.R.W.; Moazzen-Ahmadi, N. High resolution infrared spectroscopy of carbon dioxide clusters up to $(CO_2)_{13}$. *J. Chem. Phys.* **2011**, *135*, 044315. [CrossRef]
41. Bödecker, M.; Mihrin, D.; Suhm, M.A.; Wugt Larsen, R. Regularities and Anomalies in Neon Matrix Shifts of Hydrogen-Bonded O–H Stretching Fundamentals. *J. Phys. Chem. A* **2024**, *128*, 7124–7136. [CrossRef] [PubMed]
42. Andersen, J.; Heimdal, J.; Mahler, D.W.; Nelander, B.; Wugt Larsen, R. Communication: THz absorption spectrum of the CO_2–H_2O complex: Observation and assignment of intermolecular van der Waals vibrations. *J. Chem. Phys.* **2014**, *140*, 091103. [CrossRef]
43. Andersen, J.; Voute, A.; Mihrin, D.; Heimdal, J.; Berg, R.W.; Torsson, M.; Wugt Larsen, R. Probing the global potential energy minimum of $(CH_2O)_2$: THz absorption spectrum of $(CH_2O)_2$ in solid neon and *Para*-Hydrog. *J. Chem. Phys.* **2017**, *146*, 244311. [CrossRef]
44. Andersen, J.; Heimdal, J.; Nelander, B.; Wugt Larsen, R. Competition between weak OH···π and CH···O hydrogen bonds: THz spectroscopy of the C_2H_2—H_2O and C_2H_4—H_2O complexes. *J. Chem. Phys.* **2017**, *146*, 194302. [CrossRef]

45. Soulard, P.; Tremblay, B. Vibrational investigations of CO_2-H_2O, CO_2-$(H_2O)_2$, and $(CO_2)_2$-H_2O complexes isolated in solid neon. *J. Chem. Phys.* **2015**, *143*, 224311. [CrossRef]
46. Yazdabadi, S.H.; Mihrin, D.; Feilberg, K.L.; Wugt Larsen, R. Self-aggregation and microhydration mechanisms of monoethanolamine: Far-infrared identification of large-amplitude hydrogen bond libration. *J. Chem. Phys.* **2024**, *161*, 154301. [CrossRef]
47. Soulard, P.; Tremblay, B. Matrix infrared spectroscopic and ab initio investigations of methylamine-CO_2 and methylamine-CO_2-water complexes. *J. Mol. Struct.* **2023**, *1288*, 135777. [CrossRef]
48. Brauman, J.I.; Riveros, J.M.; Blair, L.K. Gas-phase basicities of amines. *J. Am. Chem. Soc.* **1971**, *93*, 3914–3916. [CrossRef]
49. Headley, A.D. Substituent effects on the basicity of dimethylamines. *J. Am. Chem. Soc.* **1987**, *109*, 2347–2348. [CrossRef]
50. Mihrin, D.; Feilberg, K.L.; Wugt Larsen, R. Self-Association and Microhydration of Phenol: Identification of Large-Amplitude Hydrogen Bond Librational Modes. *Molecules* **2024**, *29*, 3012. [CrossRef]
51. Mihrin, D.; Voute, A.; Jakobsen, P.W.; Feilberg, K.L.; Wugt Larsen, R. The effect of alkylation on the micro-solvation of ethers revealed by highly localized water librational motion. *J. Chem. Phys.* **2022**, *156*, 084305. [CrossRef]
52. Mihrin, D.; Andersen, J.; Jakobsen, P.W.; Wugt Larsen, R. Highly localized H_2O librational motion as a far-infrared spectroscopic probe for microsolvation of organic molecules. *Phys. Chem. Chem. Phys.* **2019**, *21*, 1717–1723. [CrossRef]
53. Andersen, J.; Heimdal, J.; Wugt Larsen, R. The influence of large-amplitude librational motion on the hydrogen bond energy for alcohol—water complexes. *Phys. Chem. Chem. Phys.* **2015**, *17*, 23761–23769. [CrossRef]
54. Heger, M.; Andersen, J.; Suhm, M.A.; Wugt Larsen, R. The donor OH stretching–libration dynamics of hydrogen-bonded methanol dimers in cryogenic matrices. *Phys. Chem. Chem. Phys.* **2016**, *18*, 3739–3745. [CrossRef]
55. Pracht, P.; Bohle, F.; Grimme, S. Automated exploration of the low-energy chemical space with fast quantum chemical methods. *Phys. Chem. Chem. Phys.* **2020**, *22*, 7169–7192. [CrossRef]
56. Neese, F.; Wennmohs, F.; Becker, U.; Riplinger, C. The ORCA quantum chemistry program package. *J. Chem. Phys.* **2020**, *152*, 224108. [CrossRef]
57. Neese, F. Software update: The ORCA program system—Version 5.0. *Wiley Interdiscip. Rev. Comput. Mol. Sci.* **2022**, *12*, e1606. [CrossRef]
58. Neese, F. The SHARK integral generation and digestion system. *J. Comput. Chem.* **2022**, *44*, 381–396. [CrossRef]
59. DTU Computing Center. *DTU Computing Center Resources*; Technical University of Denmark: Kongens Lyngby, Denmark, 2024. [CrossRef]
60. Bannwarth, C.; Ehlert, S.; Grimme, S. GFN2-xTB—An Accurate and Broadly Parametrized Self-Consistent Tight-Binding Quantum Chemical Method with Multipole Electrostatics and Density-Dependent Dispersion Contributions. *J. Chem. Theory Comput.* **2019**, *15*, 1652–1671. [CrossRef]
61. Stephens, P.J.; Devlin, F.J.; Chabalowski, C.F.; Frisch, M.J. Ab initio calculation of vibrational absorption and circular dichroism spectra using density functional force fields. *J. Phys. Chem.* **1994**, *98*, 11623–11627. [CrossRef]
62. Caldeweyher, E.; Ehlert, S.; Hansen, A.; Neugebauer, H.; Spicher, S.; Bannwarth, C.; Grimme, S. A generally applicable atomic-charge dependent London dispersion correction. *J. Chem. Phys.* **2019**, *150*, 154122. [CrossRef]
63. Caldeweyher, E.; Bannwarth, C.; Grimme, S. Extension of the D_3 dispersion coefficient model. *J. Chem. Phys.* **2017**, *147*, 034112. [CrossRef]
64. Neese, F.; Wennmohs, F.; Hansen, A.; Becker, U. Efficient, approximate and parallel Hartree–Fock and hybrid DFT calculations. A 'chain-of-spheres' algorithm for the Hartree–Fock exchange. *Chem. Phys.* **2009**, *356*, 98–109. [CrossRef]
65. Helmich-Paris, B.; de Souza, B.; Neese, F.; Izsák, R. An improved chain of spheres for exchange algorithm. *J. Chem. Phys.* **2021**, *155*, 104109. [CrossRef]
66. Kossmann, S.; Neese, F. Efficient Structure Optimization with Second-Order Many-Body Perturbation Theory: The RIJCOSX-MP2 Method. *J. Chem. Theory Comput.* **2010**, *6*, 2325–2338. [CrossRef]
67. Bernholdt, D.E.; Harrison, R.J. Large-scale correlated electronic structure calculations: The RI-MP2 method on parallel computers. *Chem. Phys. Lett.* **1996**, *250*, 477–484. [CrossRef]
68. Kendall, R.A.; Dunning, T.H.; Harrison, R.J. Electron affinities of the first-row atoms revisited. Systematic basis sets and wave functions. *J. Chem. Phys.* **1992**, *96*, 6796–6806. [CrossRef]
69. Neese, F. An improvement of the resolution of the identity approximation for the formation of the Coulomb matrix. *J. Comput. Chem.* **2003**, *24*, 1740–1747. [CrossRef]
70. Neese, F.; Wennmohs, F.; Hansen, A. Efficient and accurate local approximations to coupled-electron pair approaches: An attempt to revive the pair natural orbital method. *J. Chem. Phys.* **2009**, *130*, 114108. [CrossRef]
71. Riplinger, C.; Sandhoefer, B.; Hansen, A.; Neese, F. Natural triple excitations in local coupled cluster calculations with pair natural orbitals. *J. Chem. Phys.* **2013**, *139*, 134101. [CrossRef]
72. Neese, F.; Hansen, A.; Liakos, D.G. Efficient and accurate approximations to the local coupled cluster singles doubles method using a truncated pair natural orbital basis. *J. Chem. Phys.* **2009**, *131*, 064103. [CrossRef]
73. Riplinger, C.; Neese, F. An efficient and near linear scaling pair natural orbital based local coupled cluster method. *J. Chem. Phys.* **2013**, *138*, 034106. [CrossRef]

74. Riplinger, C.; Pinski, P.; Becker, U.; Valeev, E.F.; Neese, F. Sparse maps—A systematic infrastructure for reduced-scaling electronic structure methods. II. Linear scaling domain based pair natural orbital coupled cluster theory. *J. Chem. Phys.* **2016**, *144*, 024109. [CrossRef] [PubMed]
75. Kossmann, S.; Neese, F. Comparison of two efficient approximate Hartee–Fock approaches. *Chem. Phys. Lett.* **2009**, *481*, 240–243. [CrossRef]
76. Liakos, D.G.; Sparta, M.; Kesharwani, M.K.; Martin, J.M.L.; Neese, F. Exploring the Accuracy Limits of Local Pair Natural Orbital Coupled-Cluster Theory. *J. Chem. Theory Comput.* **2015**, *11*, 1525–1539. [CrossRef]